Quantum control of phase fluctuations in semiconductor lasers

Christos T. Santis[a,1], Yaakov Vilenchik[a], Naresh Satyan[b], George Rakuljic[b], and Amnon Yariv[a,1]

[a]Department of Applied Physics and Materials Science, California Institute of Technology, Pasadena, CA 91125; and [b]Telaris Inc., Santa Monica, CA 90403

Contributed by Amnon Yariv, July 3, 2018 [sent for review April 19, 2018; reviewed by Mordechai (Moti) Segev and Eli Yablonovich]

Few laser systems allow access to the light–emitter interaction as versatile and direct as that afforded by semiconductor lasers. Such a level of access can be exploited for the control of the coherence and dynamic properties of the laser. Here, we demonstrate, theoretically and experimentally, the reduction of the quantum phase noise of a semiconductor laser through the direct control of the spontaneous emission into the laser mode, exercised via the precise and deterministic manipulation of the optical mode's spatial field distribution. Central to the approach is the recognition of the intimate interplay between spontaneous emission and optical loss. A method of leveraging and "walking" this fine balance to its limit is described. As a result, some two orders of magnitude reduction in quantum noise over the state of the art in semiconductor lasers, corresponding to a minimum linewidth of 1 kHz, is demonstrated. Further implications, including an additional order-of-magnitude enhancement in effective coherence by way of control of the relaxation oscillation resonance frequency and enhancement of the intrinsic immunity to optical feedback, highlight the potential of the proposed concept for next-generation, integrated coherent systems.

semiconductor laser | spontaneous emission | temporal coherence | phase noise | optical resonator

Spontaneous emission is central to the laser process, serving as both seed and fundamental limit to the laser light's temporal coherence (1, 2). A balancing act of minimizing spontaneous emission noise while keeping sufficient gain for oscillation is called for in the continual push for increased performance, especially in the face of increasingly constraining technological requirements (e.g., size and complexity). Such a process may also entail the challenging of long-held notions on laser design and will certainly require the constant awareness of the intimate interplay between spontaneous emission, optical loss, and population inversion.

The last couple decades have seen a flurry of research activity around the control of spontaneous emission based on the principles first prescribed by E. M. Purcell (3). Innovative ideas in areas such as photonic bandgap engineering and optical confinement (i.e., resonators), coupled with progress in materials and fabrication technology, have enabled an unprecedented level of control over light–emitter interaction (4–6). Both suppression and enhancement of spontaneous emission have been demonstrated, with implications ranging from threshold reduction (i.e., thresholdless laser), radiative efficiency, and modulation bandwidth enhancement in microcavity semiconductor lasers to nonclassical light generation (e.g., sub-Poissonian and amplitude-squeezed light) (7–9), but never, to the best of our knowledge, for the express purpose of enhancing laser coherence. A small number of theoretical investigations into the effect of spontaneous emission modification on the linewidth of microcavity semiconductor lasers by way of cavity size control has failed to produce a consensus as to whether it should lead to a narrowing or broadening of linewidth, presumably due to conflicting assumptions regarding other contributing parameters (e.g., threshold) (10, 11).

Here, we demonstrate, theoretically and experimentally, the control of spontaneous emission into the laser mode of a semiconductor laser for the purpose of suppressing quantum noise and enhancing its temporal coherence. The control is exercised through the direct and precise manipulation of the mode's spatial field distribution (i.e., modal control) relative to the emitter [i.e., quantum well (QW)]. It is technically implemented in a seamless fashion, without change in cavity size or use of external elements. Harnessing recent advancements in photonic integration [i.e., silicon (Si)/III-V] and optical resonator design, some two orders of magnitude improvement in the coherence of semiconductor laser over the state of the art is achieved.

In what follows, we begin by reviewing, for the sake of completeness, the main mechanisms involved in quantum noise as they pertain to a semiconductor laser and laying out the theoretical premise of our approach: the direct, modal control of spontaneous emission into the laser mode. The latter is then applied to the case of a real laser system, a Si/III-V semiconductor laser. Numerical modeling and theoretical performance estimates are followed by experimental results of fabricated lasers. The paper concludes with a discussion on the merits, limitations, and future prospects of the work.

Theoretical Background

The theoretical basis of our approach is the phase diffusion model for a stochastic noise-driven laser oscillator (2). Despite its simplicity, it encompasses the main mechanisms at work and provides quick insight into their interplay. Fundamentally, the

Significance

The semiconductor laser, arguably the most versatile member of the family of lasers, has become a technological staple of a massively interconnected, data-driven world, with its spectral purity (i.e., temporal coherence) an increasingly important figure of merit. The present work describes a conceptually fundamental "recipe" for the enhancement of coherence, predicated on direct control of the coherence-limiting process itself, the field–matter interaction. As such, it is inherently adaptable and technologically scalable. As photonic materials and fabrication techniques continue to improve, the described approach has the potential of serving as a roadmap for major and sustained improvements in coherence. With experimentally demonstrated coherence limited at 1 kHz in this work, we envision "deep" sub-kilohertz-level coherence to be soon within reach.

Author contributions: C.T.S., Y.V., N.S., G.R., and A.Y. designed research; C.T.S., Y.V., and N.S. performed research; C.T.S., Y.V., and N.S. analyzed data; and C.T.S. and A.Y. wrote the paper.

Reviewers: M.S., Technion-Israel Institute of Technology; and E.Y., University of California, Berkeley.

The authors declare no conflict of interest.

This open access article is distributed under Creative Commons Attribution-NonCommercial-NoDerivatives License 4.0 (CC BY-NC-ND).

[1]To whom correspondence may be addressed. Email: ayariv@caltech.edu or christos@caltech.edu.

Published online August 7, 2018.

temporal coherence of laser emission is limited by phase noise, the result of zero-point (i.e. vacuum) fluctuations of the laser field (12, 13). Atoms, in general, or electrons in the case of a semiconductor laser, interacting with these fluctuations undergo "spontaneous" transitions from excited to lower-lying energy states, emitting in the process photons with phases uncorrelated with that of the coherent field. Under the effect of a large number of such events, the optical phase of the field, θ, performs a random, diffusion-type "walk" in the complex phasor plane accumulating a variance

$$\left\langle \Delta\theta(\tau)^2 \right\rangle = \frac{N_{2t}\, W_{sp}^{(\ell)}}{2n_\ell}(1+\alpha^2)\tau, \qquad [1]$$

over time τ. It is this phase excursion that is the pertinent figure of merit for performance in many practical applications, such as, for example, optical coherent communications, τ in that case being the duration of a single symbol of information (14).

In Eq. **1**, $W_{sp}^{(\ell)}$ is the spontaneous emission rate (in s^{-1}) per electron into the laser mode, denoted by "ℓ"; N_{2t} is the total number of electrons in the excited level (i.e., conduction band), clamped at its threshold value; and n_ℓ is the number of light quanta stored in the laser mode. The linewidth enhancement factor α accounts for the excess phase noise due to coupling between amplitude and phase fluctuations and will be treated here as a constant. The product $N_{2t}\, W_{sp}^{(\ell)}$ represents the total spontaneous emission rate, $R_{sp}^{(\ell)}$ (in photons per second), into the laser mode. The energy due to n_ℓ coherent quanta in the laser mode, proportional to the photon lifetime in the cavity, acts as an optical "flywheel" which resists the spontaneous emission-driven diffusion of the phase. The three quantities, $W_{sp}^{(\ell)}$, N_{2t}, and n_ℓ, are implicitly coupled through the quantized nature of the electromagnetic (EM) field, optical resonator fundamentals, and semiconductor physics.

As our approach to the suppression of quantum noise relies on the modal control of the spontaneous emission into the laser mode, it is advantageous to express the laser field as an expansion in normal modes (15, 16), the eigenmodes of the resonator,

$$\bar{\mathscr{E}}(\bar{r}, t) = -\sum_s \frac{1}{\sqrt{\epsilon(r)}} p_s(t)\bar{E}_s(\bar{r}), \qquad [2]$$

$$\bar{\mathscr{H}}(\bar{r}, t) = \sum_s \frac{1}{\sqrt{\mu(r)}} \omega_s q_s(t)\bar{H}_s(\bar{r}), \qquad [3]$$

where mode functions E_s,H_s are exact solutions of Maxwell's equations for the specific resonator and subject to orthogonality and normalization conditions

$$\int_{V_c} \bar{E}_s(\bar{r}) \cdot \bar{E}_t(\bar{r})\, d^3\bar{r} = \delta_{s,t}, \qquad [4]$$

$$\int_{V_c} \bar{H}_s(\bar{r}) \cdot \bar{H}_t(\bar{r})\, d^3\bar{r} = \delta_{s,t}, \qquad [5]$$

where V_c is the cavity volume. The quantization of the field comes about naturally through the association of the expansion coefficients, p_s and q_s, of each mode with the momentum and coordinate operators, respectively, of a quantum mechanical oscillator.

Application of time-dependent perturbation theory to the interaction of an electron, located at a position in the laser's active region denoted by $\bar{r}_a$, with the quantized field yields expressions for the spontaneous and stimulated transition rates of an electron from an excited state in the conduction band to an unoccupied state in the valence band (i.e., hole), by which a photon is emitted into mode (ℓ),

$$W_{sp}^{(\ell)} = \frac{2\pi^2\mu^2\nu_\ell g_a(\nu_\ell)}{h\epsilon(r_a)}|\bar{E}_\ell(\bar{r}_a)|^2, \qquad [6]$$

$$W_{st}^{(\ell)} = n_\ell\, W_{sp}^{(\ell)}, \qquad [7]$$

where μ is the dipole transition matrix element and $g_a(\nu_\ell)$ (in units of s) the value of the normalized lineshape function of the transition at the lasing frequency ν_ℓ, both known quantities for our purposes, and $|\bar{E}_\ell(\bar{r}_a)|^2$ is the normalized intensity of the laser mode at the location of the emitter (i.e., electron).

The latter constitutes a modal "knob" on the rate of spontaneous emission into the laser mode. On a more fundamental, quantum-mechanical level, it can be shown that the field's quantum fluctuations, the root cause of noise, bear the spatial signature of each constituent mode and, through it, information about the size, shape, and overall structure of the resonator (*Appendix A*). Therein lies the guiding insight toward quantum noise reduction. Instead of the brute-force method of reducing $|\bar{E}_\ell(\bar{r}_a)|^2$, the quantum fluctuations intensity, by "dilution" of the zero-point energy through increase of the mode volume, we achieve the same result by a subtle, modal engineering which leaves the mode profile essentially unaltered.

It may seem straightforward, at first, to try to suppress noise by an arbitrary reduction of $|\bar{E}_\ell(\bar{r}_a)|^2$. However, it follows from Eq. **7** that any attempt to reduce the spontaneous emission rate into laser mode (ℓ) will have a proportionally similar effect on the stimulated rate and, thus, on the laser gain needed to overcome losses, thus forcing the laser medium to a higher inversion point (i.e., higher N_{2t}). This will not only cause the threshold to increase, but also cut into, or even negate, any expected reduction in noise. One way to break this conundrum and create positive leverage for the reduction of quantum noise is by linking any decrease in spontaneous emission rate to a commensurate decrease in the optical loss rate, thus keeping the threshold current effectively unchanged (see *Appendix D* for more on this).

The laser architecture for high coherence, introduced here, constitutes a departure from long-standing conventions of semiconductor laser design. Semiconductor laser designs typically seek to maximize the modal overlap with the active region (QW) and, thereby, the available modal gain (Fig. 1*A*). This choice, however, is attendant upon a significant loss (e.g., free-carrier absorption) and, thus, noise. It also leaves no room for internally manipulating $|\bar{E}_\ell(\bar{r}_a)|^2$, as the active region is surrounded by highly absorbing and low-index regions. By contrast, placing the active region in close proximity to a high-index, low-loss layer, as shown in Fig. 1*B*, creates the potential for direct control of $|\bar{E}_\ell(\bar{r}_a)|^2$ by modal engineering in tandem with loss reduction. The decrease in modal gain brought about by the reduction of $|\bar{E}_\ell(\bar{r}_a)|^2$ is offset by a decrease in loss by virtue of increased confinement in the lower-loss layer, thus keeping the threshold current practically constant. This, of course, cannot go on indefinitely. The point to which this balance can be maintained defines the useful margin for noise reduction and is determined by the point where loss in the low-loss, guiding layer starts to become the dominant modal loss and, thus, the limiting factor of the total loss, foreshadowing the role of this layer as a figure of merit for coherence.

Design and Analysis

The practical realization of the concepts described above draws upon recent advancements in the area of photonic integration and, specifically, the heterogeneous integration of Si and III-V

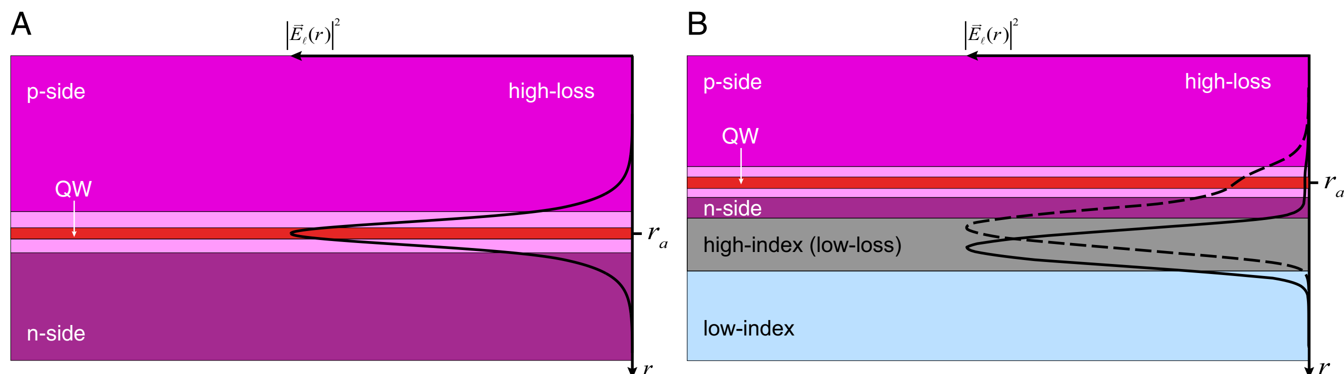

Fig. 1. Concept illustration of the modal control of spontaneous emission in a semiconductor laser. (*A*) Cross-sectional structure of a generic, electrically pumped semiconductor laser along with a simulated example of the transverse distribution of the electric field intensity, $|\bar{E}_\ell(\bar{r})|^2$, of the laser mode. (*B*) In a departure from the standard semiconductor laser design, the laser mode is "pulled" into and is guided by a transversely proximal to the active region layer. The low-loss nature of the latter is key for offsetting the resulting decrease in modal gain. The location of the active region in the evanescent tail of the mode enables leveraged (i.e., exponential) control over $|\bar{E}_\ell(\bar{r})|^2$ and, thereby, of the spontaneous emission rate into the laser mode, as showcased by two simulated examples (solid and dashed black lines).

(i.e., InP) (17). Si provides the requisite low-loss, guiding layer, bringing along a proven set of methods for the design and fabrication of low-loss, optical structures (e.g., waveguides, gratings, resonators, etc.) (18, 19). In a key addition to the standard Si/III-V laser structure, we introduce a relatively thick, up to $\sim$150 nm, layer of silica (SiO_2) between the Si and the III-V, shown in Fig. 2 *A* and *B*. The thickness of this layer, controllable on a nanometer scale, offers a precise and leveraged means of control of $|\bar{E}_\ell(\bar{r}_a)|^2$ and, thus, of the rate of spontaneous emission, as illustrated by simulated examples in Fig. 2 *C* and *D*. For short and for its distinct role, this layer will be referred to as the quantum noise control layer (QNCL).

Loss control is central to the scheme, as explained above, and, thus, warrants a closer look. For a consistent description of the overall loss and its constituent components, we use the cold cavity quality factor (Q). In the limit of low confinement in the III-V, as is the case for the lasers in this work (i.e., $\Gamma_{\text{III-V}}<10\%$), the total Q (i.e., loaded) can be written as

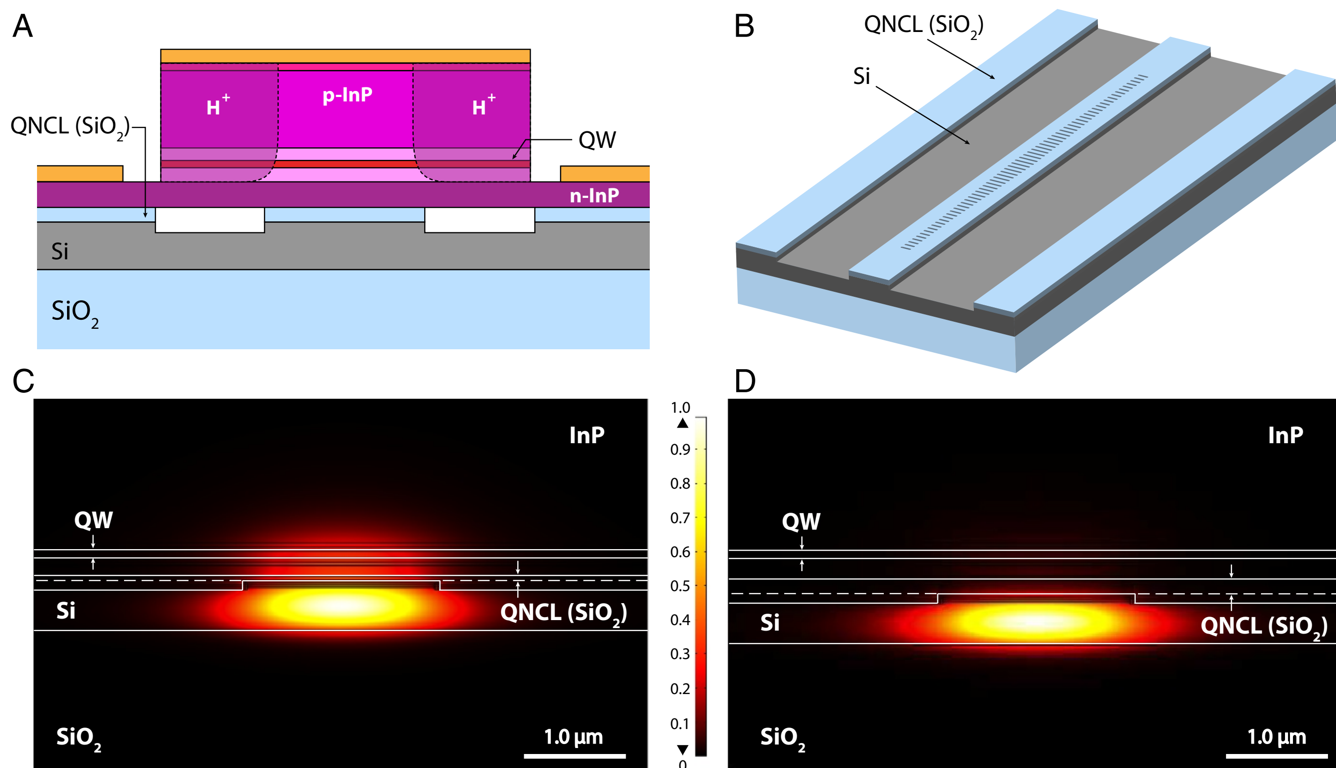

Fig. 2. Spontaneous emission control on Si/III-V platform. (*A*) Cross-sectional structure of a Si/III-V laser featuring a SiO_2 spacer layer (QNCL) between Si and III-V for the modal control of the spontaneous emission rate into the laser mode. (*B*) A 3D schematic of the optical resonator (III-V omitted for clarity). Note that the design of the resonator accounts for the presence of the III-V (i.e., hybrid resonator). (*C* and *D*) Simulated examples of the spatial (2D) distribution of the (normalized) amplitude of the electric field ($|\bar{E}_\ell(\bar{r})|$) of the laser mode (TE_0) for two extreme cases of QNCL thickness—50 nm (*C*) and 200 nm (*D*)—representing a more than an order-of-magnitude swing in the rate of spontaneous emission.

$$\frac{1}{\mathrm{Q}} = \frac{1}{\mathrm{Q}_{\mathrm{III-V}}} + \frac{1}{\mathrm{Q}_{\mathrm{Si}}} + \frac{1}{\mathrm{Q}_{\mathrm{e}}}, \qquad [8]$$

where Q_{Si} accounts for loss to scattering, predominantly in Si; $\mathrm{Q}_{\mathrm{III-V}}$ accounts for loss to (free-carrier) absorption, predominantly in the III-V; and Q_{e} accounts for loss to the useful output. As $\mathrm{Q}_{\mathrm{III-V}}$ depends on the modal intensity in the III-V (*Appendix C*), including that in the active region, a key codependence between III-V loss and spontaneous emission exists. This relation can be harnessed for the purpose of noise reduction as long as $\mathrm{Q}_{\mathrm{III-V}} \ll \mathrm{Q}_{\mathrm{Si}}, \mathrm{Q}_{\mathrm{e}}$. To maximize the useful margin for noise reduction, Q_{Si} has to be maximized as well (Q_{e} is designer-controlled and can be set at will). This is done by resonator design and optimization of the fabrication process (20, 21). The benchmark value of Q_{Si} in this work is $\sim 10^6$ (intrinsic).

We now return to the metric for coherence, as defined in Eq. **1**, or, equivalently, its associated spectral linewidth $\left[\Delta\nu = (2\pi\tau)^{-1} \left\langle \Delta\theta(\tau)^2 \right\rangle\right]$. Applying optical resonator and laser fundamentals (*Appendix E*), the linewidth of a semiconductor laser can be written as

$$\Delta\nu = \frac{e\mu^2\omega_\ell^2 g_a(\omega_\ell)\left(1+\alpha^2\right)}{\eta_i h \epsilon(r_a)(I - I_{th})\mathrm{Q}} \left[|\bar{E}_\ell(\bar{r}_a)|^2 N_{tr} + \frac{\omega_\ell}{g' V_a \mathrm{Q}} \right], \qquad [9]$$

where I and I_{th} are the injection and threshold currents, respectively; η_i is the internal quantum efficiency (including carrier injection efficiency); g' is a material-dependent, differential gain coefficient (in s^{-1}); and V_a is the volume of the active region. The first term in the brackets corresponds to the spontaneous emission due the N_{tr} carriers (absolute number) necessary to render the active region transparent (i.e., transparency term), whereas the second term accounts for spontaneous emission from the additional carriers injected to compensate for loss (i.e., threshold term). The former term depends on material properties only and not on the resonator, while the latter does depend on the resonator loss, hence the Q^{-1} dependence. Conversely, the transparency term depends on $|\bar{E}_\ell(\bar{r}_a)|^2$, whereas the threshold term does not, which follows from the fundamental relationship between the spontaneous and stimulated emission (Eq. **7**). The additional Q in the denominator of the prefactor is shared by both terms and reflects the dependence of the photon number, n_ℓ, on loss. For our purposes, all quantities in Eq. **9**, except for $|\bar{E}_\ell(\bar{r}_a)|^2$ and Q, are considered fixed.

Plotted in Fig. 3*A* is the relative spontaneous emission rate into the laser mode, normalized to a generic, reference semiconductor laser, for three different values of Q_{Si} and as a function of the QNCL thickness. The lasers under study in this work and the reference one are assumed to be similar in all aspects except in loss and fraction of mode confinement in the active region [i.e., $|\bar{E}_\ell(\bar{r}_a)|^2$], for which values typical of III-V semiconductor lasers are assumed for the reference laser (Fig. 3*A*). Solid lines correspond to the sum of the two spontaneous emission components, transparency $[R_{sp}^{(tr)}]$ and threshold $[R_{sp}^{(th)}]$, for each Q_{Si}, with that for $\mathrm{Q}_{\mathrm{Si}}=10^6$ further analyzed into its constituent components, shown with blue dashed lines. We find the spontaneous emission due to the transparency carrier population to decrease monotonically with the QNCL thickness due to its $|\bar{E}_\ell(\bar{r}_a)|^2$ dependence, whereas that due to threshold population levels off as a result of the saturation of Q to the respective Q_{Si} value. For a given Q_{Si}, we can define two distinct regimes for the total spontaneous emission into the laser mode: a transparency-limited regime which obtains with "thinner" QNCLs [i.e., larger $|\bar{E}_\ell(\bar{r}_a)|^2$] and a threshold-limited one at "thicker" QNCLs. The inflection point on each trace marking the boundary between the two regimes occurs at the point where absorption loss in the

APPLIED PHYSICAL SCIENCES

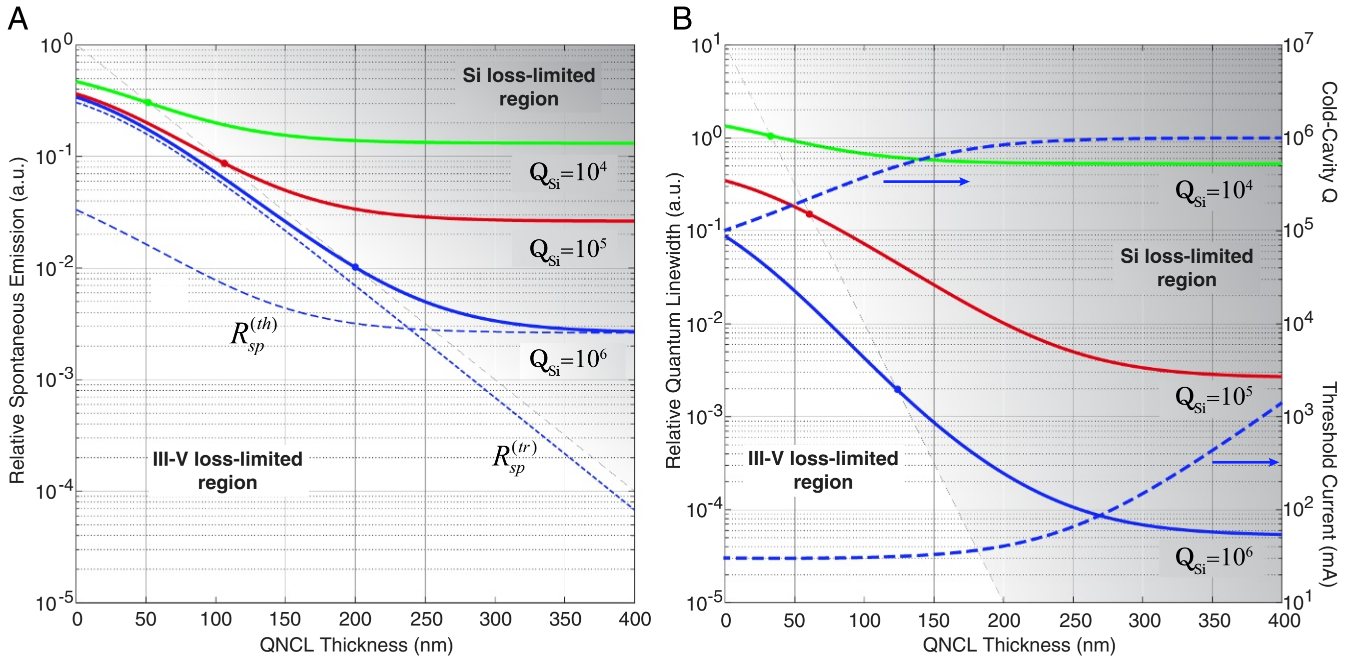

Fig. 3. Numerical analysis and performance estimates. (*A*) Relative spontaneous emission rate into the laser mode, normalized with respect to a generic semiconductor laser (parameters listed below), as a function of QNCL thickness and for three different values of Q_{Si} (solid lines). Blue dashed lines correspond to the individual spontaneous emission components, $R_{sp}^{(tr)}$ and $R_{sp}^{(th)}$, respectively, for the case of $\mathrm{Q}_{\mathrm{Si}}=10^6$. (*B*) Relative quantum linewidth calculated for the same parameters as those of *A*. Also plotted in dashed lines are the threshold current and cold cavity Q as a function of QNCL thickness for $\mathrm{Q}_{\mathrm{Si}}=10^6$. Gray-shaded regions in both images illustrate the combined area corresponding to the Si loss-limited regime for all possible values of QNCL. The boundary between the Si and III-V loss-limited regions is formed by the locus of the inflection point of each curve. The reference semiconductor laser used in the normalization is taken to have an active region of volume similar to that of the Si/III-V lasers of this work, V_a=(L×W×H) = (1 mm×10 μm×40 nm), a mode confinement factor of $\Gamma_{\mathrm{QW}} = 10\%$, a differential gain coefficient of $g' = 4 \times 10^{-15}\ \mathrm{s}^{-1}$, and modal loss equivalent to a loaded Q of 10^4.

III-V equals the combined loss to other channels, namely, scattering (Q_{Si}) and output (Q_e). Clearly, operating beyond this point bears increasingly diminishing returns as far as spontaneous emission reduction. The optimal point moves to thicker QNCLs with increasing Q_{Si}, allowing an increasingly wider margin for spontaneous emission reduction. As an example, an increase in Q_{Si} from 10^4, typical of all-III-V semiconductor lasers, to 10^6 creates a nearly two-order-of-magnitude additional potential for spontaneous emission reduction, highlighting the role of Q_{Si} as a figure of merit for coherence.

Plotted in Fig. 3*B* is the respective normalized quantum linewidth for each case of Q_{Si}. The qualitative trend as a function of the QNCL thickness remains the same as that of Fig. 3*A*, but the vertical scale has now grown, accounting for the additional contribution from the Q factor in the denominator Eq. **9**. An additional two-order-of-magnitude margin for linewidth reduction between $Q_{Si}=10^4$ and 10^6 is created by the photon lifetime enhancement alone, bringing the aggregate margin to 10^4. The "weight" of Q and its saturation effect have also been enhanced as a result, moving the inflection points on each trace to smaller QNCL thicknesses. An alternative criterion for the transition into the Si loss-limited regime can be defined in terms of the threshold current. Also plotted in Fig. 3*B* in blue dashed lines are the cold cavity Q and threshold current as a function of QNCL thickness for $Q_{Si}=10^6$. The latter remains practically constant throughout the III-V loss-limited region and starts to rise rapidly upon the onset of the Q saturation (i.e., Si loss-limited regime). Gray shading in Fig. 3 is used to delineate the Si from the III-V loss-limited regime in the design parameter space.

Experiment

Fabricated lasers were characterized for their coherence and, specifically, the quantum limit imposed on it by spontaneous emission (more on fabrication and characterization is provided in *Materials and Methods*). To resolve the signature of spontaneous emission on the lasers' coherence and separate it from that of technical noise (e.g., temperature or electronic), we measured the full frequency noise spectrum. This measurement becomes increasingly necessary, but also challenging, as quantum noise is suppressed. Noise due to spontaneous emission manifests itself in the frequency noise spectrum as a white noise plateau at high frequencies (>100 kHz), where contributions from technical and $1/f$ noise have dropped to relative unimportance.

Plotted in Fig. 4*A* is the power spectral density (PSD) (in units of equivalent white noise linewidth, $\pi\text{Hz}^2/\text{Hz}$) of the frequency noise of Si/III-V lasers with three different QNCL thicknesses, 30, 100, and 150 nm, which are expected to span the breadth of the III-V loss-limited regime for $Q_{Si}=10^6$. Plotted along is the frequency noise of a commercial distributed feedback (DFB) laser (JDSU model no. CQF935/808), used for measurement calibration and comparison. All traces, with the exception of that of the reference DFB, correspond to measurements taken at the same current increment above each laser's respective threshold, in an effort to cancel out any variation in noise between lasers due to pumping. A clear trend of decreasing level of quantum noise with increasing QNCL thickness, indicative of decreasing spontaneous emission noise, is observed. The quantum-limited linewidths, extracted at the minimum frequency noise point (~200 MHz), are 35, 2.5, and 1.3 kHz for the

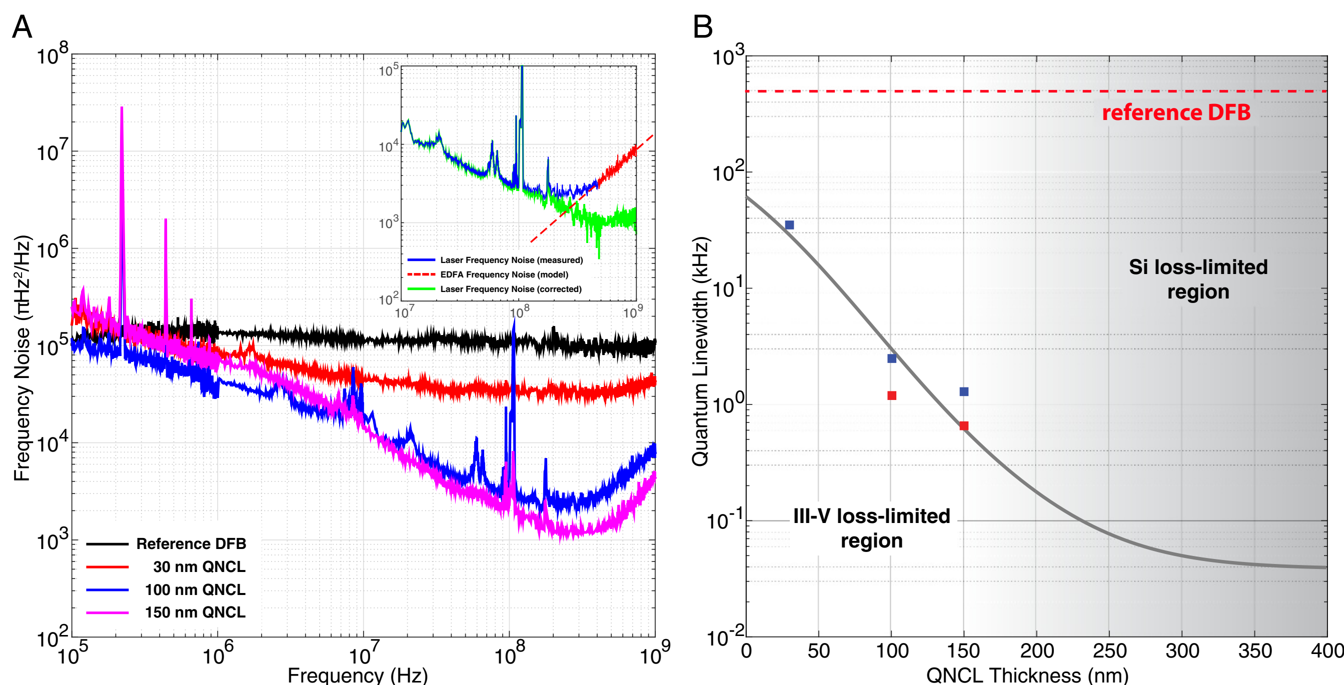

Fig. 4. Experimental results. (*A*) Measured PSD (in units of equivalent white noise linewidth, $\pi\text{Hz}^2/\text{Hz}$) of the frequency noise of Si/III-V lasers with three different values of QNCL thickness (30, 100, and 150 nm). Plotted alongside for comparison is the frequency noise spectrum of a commercial DFB (black trace), also used for measurement calibration. All the traces of the Si/III-V lasers were taken at the same current increment (~30 mA) from their respective threshold, while that of the reference DFB was at its maximum operating current. (*A*, *Inset*) Numerical correction for the EDFA noise for the case of the 100 nm QNCL. The measured noise above ~300 MHz is fitted to $S_{\Delta\nu}(f)=af^b+S_o$ (red dashed line), with a, b being fitting coefficients and S_o a frequency-independent term (i.e., white noise). Subtracting the frequency-dependent term (i.e., af^b) from the measured noise yields the corrected spectrum (green line). (*B*) Experimental quantum linewidths (blue markers) plotted against the theoretical trend line (gray trace), as calculated via Eq. **9** for $Q_{Si}=10^6$. To set the vertical axis, the linewidth of the reference DFB (red dashed line), measured at an equivalent pump rate, is used to convert from relative (Fig. 3*B*) to absolute linewidth. Red markers represent linewidth estimates for the cases of the numerically filtered EDFA noise. The gray-shaded area corresponds to the theoretically estimated Si loss-limited region.

three lasers in descending thickness order. By comparison, the reference DFB, measured at its maximum pump level, reaches a minimum linewidth of ∼100 kHz.

It should be noted that while a clear white noise floor is recovered for the reference DFB and 30-nm QNCL laser, a less definitive picture is obtained for the 100- and 150-nm QNCLs. As the quantum noise level is "pushed" lower, both internally and externally imposed noise floors begin to surface at intermediate- and high-offset frequencies. As a result, the encounter with the white noise floor is pushed to higher frequencies, where the sensitivity of the measurement quickly degrades, rendering the results more ambiguous. In this case, we find noise injected by the Erbium-doped fiber amplifier (EDFA) used for the amplification of the fiber-coupled light to mask the quantum noise at high offset frequencies, as evidenced by the rise in frequency noise in the spectrum of the 100- and 150-nm QNCLs above ∼200 MHz. In an effort to obtain an estimate for the lasers' intrinsic linewidth, we correct for the injected noise by numerically fitting the rising part of the noise spectrum and subtracting its frequency-dependent component from the measured noise, thereby leaving any white noise content unaffected. A white noise plateau is recovered in both cases, shown for illustration for the case of the 100-nm QNCL in Fig. 4*A*, *Inset* with numerically extracted estimates for the quantum linewidths of 1.5 and 500 Hz for the 100- and 150-nm QNCL lasers, respectively.

The experimental results are compared with the theoretical predictions of the preceding section. Plotted in Fig. 4*B* are the experimental quantum linewidths of the three QNCL lasers along with the theoretically expected trend line for the case of $Q_{Si} = 10^6$, as calculated from equation Eq. **9** and presented in Fig. 3*B*. For the conversion from relative to absolute linewidth, we use the quantum linewidth of the reference DFB (∼500 kHz), measured at the same current increment from threshold as the QNCL lasers. With the exception of the data point for the 150-nm QNCL, presumably due to the effect of the noise from the EDFA, the experimental results follow the theoretical trend with reasonable agreement. When compared at the same current increment from threshold, the QNCL lasers attain a coherence level more than two orders of magnitude higher than that of the reference DBF (red dashed line in Fig. 4).

The threshold currents of the three QNCL lasers are 40, 42.5, and 47 mA for the 30-, 100-, and 150-nm QNCL, respectively. These values fall within the margin of fabrication-induced variation for the threshold current, confirming our expectation of the three chosen QNCLs lying in the III-V loss-limited regime. The output power levels of the lasers are generally low, at ∼1 mW (in-fiber, single-facet), hence the need for the EDFA. This is, in part, due to the unintended undercoupling of resonators (i.e., too high Q_e), which results in reduced output coupling efficiency, compounding the drop in efficiency due to early thermal roll-off, a well-documented occurrence in Si/III-V lasers (22). Finally, the mode confinement factors in the various regions of interest along with the quantum-limited linewidths for the three cases are summarized in Table 1.

Table 1. Calculated mode confinement factors (in %) in various regions of interest (i.e., III-V, QW, and Si) for lasers with different QNCL thickness, along with the respective measured and numerically adjusted quantum linewidths

QNCL, nm	III-V, %	QW, %	Si, %	$\Delta\nu$, kHz (exp.)	$\Delta\nu$, kHz (num.)
30	15.0	2.0	82	35.0	—
100	4.0	0.6	92	2.5	1.0
150	1.5	0.2	95	1.1	0.5

Discussion

The linewidth narrowing by the control of the spontaneous emission in our laser raises the question of the relation to the Purcell effect (3). In Purcell's original scenario, the emitter (i.e., spin) interacts with the single mode of a "closed" resonator. This is due to the fact that the resonator dimensions are on the order of the wavelength of the EM field ($V_c \sim \lambda^3$), and only one mode exists within the natural linewidth of the spin transition. In this case, the spontaneous emission rate into the mode and the total spontaneous emission rate, the inverse of the excited spin lifetime, are one and the same. In our case, the "open" structure of the resonator and the large natural linewidth ($>10^{12}$ Hz) allow the inverted electron population to emit spontaneously into a very large number of those "big-box," vacuum modes. Under these circumstances, our "surgical" control, by orders of magnitude, of the spontaneous emission rate into the laser mode has but a negligible effect on the overall spontaneous lifetime. Our spontaneous emission control can, thus, be viewed as a special case of the generalized Purcell control. Our basic results and formalism lead readily to Purcell's results under a similar set of resonator mode and transition characteristics (see *Appendix B* for more details).

A study of Eq. **9** raises the question of how far can we reduce $\Delta\nu$ by controlling $|\bar{E}_\ell(\bar{r}_a)|^2$ or, in other words, of the ultimate limit in coherence. The some-two-orders-of-magnitude reduction in $\Delta\nu$ reported in this work is reached under the condition whereby the dominant loss is optical absorption in the III-V material (i.e., $Q_{III-V} \ll Q_{Si}$). So, it is Q_{Si} that sets the limit on coherence. The question can, thus, be rephrased into how large can Q_{Si} be made. Under the experimental condition of this work, Q_{Si} is limited at $\sim 10^6$ by scattering loss, absorption loss in bulk Si being much smaller. However, if scattering loss were suppressed and/or under conditions of high intracavity power, Q_{Si} could attain a nonlinear (i.e., intensity-dependent) term due to two-photon and ensuing free-carrier absorption in Si ($\lambda < 2.2\ \mu$m), which would then become the Q_{Si}- and, ultimately, coherence-limiting factor. For the lasers of this work, the limit in coherence in terms of quantum linewidth is estimated to be in the ballpark of a few hundred hertz (23, 24). Overcoming this limit would require replacing Si with a wider-bandgap material.

Lastly, the control of the field–emitter interaction and optical loss proposed and achieved in this work has additional performance implications. A laser operating with a high loaded (cold cavity) Q factor is expected to exhibit inherent robustness against the detrimental effects of external back-reflections (i.e., coherence collapse) by virtue of enhanced effective mirror reflectivity (i.e., high Q_e). A laser with intrinsic, relative immunity to optical feedback high enough to obviate the need for an optical isolator can, thus, be envisioned. Finally, the reduction of the spontaneous emission rate into the laser mode, coupled with the enhancement of photon lifetime, enables substantial, up to an order of magnitude reduction in the relaxation oscillation resonance frequency, thereby enhancing the effective short-term coherence by suppressing the contribution from carrier noise through amplitude-to-phase fluctuation coupling at offset frequencies of importance for many practical applications (e.g., Gb/s-rate coherent communications). These prospects highlight further the potential of a laser embodying the described concepts as a powering source of next-generation, chip-scale, coherent solutions.

Appendices

Appendix A: EM Field Mode-Expansion and Quantization. Substituting the field mode expansions (2) and (3) in the expression for the field's Hamiltonian and applying the normalization conditions (4) and (5) yields

APPLIED PHYSICAL SCIENCES

$$\mathcal{H} = \frac{1}{2}\sum_s \left(p_s^2 + \omega_s^2 q_s^2\right), \quad [10]$$

which has the form of a sum of Hamiltonians of independent (classical) harmonic oscillators. The quantization of the EM field, then, comes about naturally by associating the expansion coefficients, p_s, q_s, with the momentum and coordinate operators, respectively, of a quantum mechanical oscillator. Subject to the appropriate commutation relations, time-dependent boson operators, $\alpha_s^\dagger, \alpha_s$, can be defined for each eigenmode in terms of its canonical variables, p_s, q_s, yielding the quantized EM field operators

$$\bar{\mathscr{E}}(\bar{r}, t) = -i\sqrt{\frac{\hbar\omega_\ell}{2\epsilon}}\sum_s \left[\alpha_s^\dagger(t) - \alpha_s(t)\right]\bar{E}_s(\bar{r}), \quad [11]$$

$$\bar{\mathscr{H}}(\bar{r}, t) = \sqrt{\frac{\hbar\omega_\ell}{2\mu}}\sum_s \left[\alpha_s^\dagger(t) + \alpha_s(t)\right]\bar{H}_s(\bar{r}). \quad [12]$$

The probabilities of the various optical transitions are derived by application of time-dependent perturbation theory and using the interaction Hamiltonian,

$$\mathcal{H}_{\text{int}} = -e\bar{r}\cdot\bar{\mathscr{E}}(\bar{r}, t), \quad [13]$$

in the dipole approximation for the interaction of the EM field with an electron-hole pair in a semiconductor medium, where $\bar{r}$ is the dipole position operator and $\bar{E}(\bar{r}, t)$ is the electric field operator of Eq. **11**. Due to the orthogonality of the eigenmodes (i.e., independence of harmonic oscillators), the transition rate (in s^{-1}) from an initial state in the conduction band ($|c\rangle$) to a final state in the valence band ($|v\rangle$) can be derived independently for each mode. Dropping the summation over all modes and retaining only the mode of interest—the laser mode—the respective transition rate is found to be

$$W_{tot}^{(\ell)} = \frac{2\pi}{\hbar}\left|\left\langle v, n_\ell + 1|\mathcal{H}_{\text{int}}^{(\ell)}|c, n_\ell\right\rangle\right|^2 \delta(E_c - E_v - \hbar\omega_\ell), \quad [14]$$

where n_ℓ and $n_\ell + 1$ are the number of photons in the laser mode in the initial and final states, respectively, and E_c, E_v are the energies of an electron in the conduction and a hole in the valence band, respectively. Due to the distributed nature of electronic states in the semiconductor (i.e., Fermi–Dirac), integration over all energies and both bands is performed for the total rate. For a single electron located at a position denoted by $\bar{r}_a$, the total rate (per electron) is

$$W_{tot}^{(\ell)} = (n_\ell + 1)\frac{2\pi^2\mu^2\nu_\ell g_a(\nu_\ell)}{h\epsilon(r_a)}|\bar{E}_\ell(\bar{r}_a)|^2, \quad [15]$$

where $\mu = \left|\left\langle v|e\bar{r}_a|c\right\rangle\right|$ is the dipole transition element and $g_a(\nu_\ell)$ is the value of the transition lineshape function—a representation of the Fermi–Dirac distribution of energies in the frequency domain—at the transition frequency ν_ℓ,

$$\int_{-\infty}^{+\infty} g_a(\nu_k)d\nu_k = 1. \quad [16]$$

Obviously, in the case of a spatially distributed ensemble of emitters (e.g., QW), the point-like modal intensity $|\bar{E}_\ell(\bar{r}_a)|^2$ is replaced with an integral over the active volume (i.e., confinement factor). The emission rate of Eq. **15** is the sum of the spontaneous ($W_{sp}^{(\ell)}$) and stimulated ($W_{st}^{(\ell)}$) emission rates of Eqs. **6** and **7**, respectively.

As already mentioned, spontaneous emission is "induced" by vacuum fluctuations of the field, the quantization of which allows us more direct insight into this obscure, quantum mechanical source. By using the expression for the quantized EM field, the magnitude of the fluctuations can be found as the variance of the field when in its vacuum state. This can, once again, be done for the laser mode independently, by virtue of the eigenmode orthogonality. As the expectation value of both field components vanishes in its vacuum state ($|0\rangle$), the variance reduces to the expectation value of the field's intensity. The intensity of the vacuum, electric field fluctuations of the laser mode, thus, becomes

$$\left(\Delta\bar{\mathscr{E}}_\ell(\bar{r})\right)^2 = \left\langle\bar{\mathscr{E}}_\ell^2(\bar{r})\right\rangle = \frac{\hbar\omega_\ell}{2\epsilon(r)}|\bar{E}_\ell(\bar{r})|^2. \quad [17]$$

The fluctuating field distribution bears the spatial signature of each eigenmode, in this particular case, the laser mode, $|\bar{E}_\ell(\bar{r})|^2$. Thus, the modal intensity provides a direct control over the quantum-mechanical, root cause of spontaneous emission.

Appendix B: Connection to the Purcell Effect. Expression Eq. **6** applies in the case where the transition linewidth, expressed by $g_a(\nu_\ell)$, is much broader than the laser mode's cold-cavity linewidth, inversely proportional to Q, a condition automatically satisfied for most semiconductors at room temperature. This regime is diametrically opposite from that considered by E. M. Purcell (3), wherein an emitter's radiative lifetime or, equivalently, its total spontaneous emission rate can be altered via modification of the optical density of states. For this to be possible, the emitter's linewidth needs to be much smaller than that of the optical mode, a condition that limits most practical applications in semiconductors to low temperatures. While control of spontaneous emission by modification of the spectral density of states may not be an option, another degree of freedom is available, the spatial modal density, represented in Eq. **6** by $|\bar{E}_\ell(\bar{r}_a)|^2$. In the operating regime of the lasers of this work, out of the potentially thousands of possible modes of a large and open-cavity resonator, the spontaneous emission rate into a specific mode—the laser mode—can be modified by control of its modal intensity, while leaving that into all other modes and, thus, the overall spontaneous emission rate largely unaffected. From that standpoint, this type of spontaneous emission control can be viewed as a special case of the Purcell effect.

In line with Purcell, we can define a factor for the suppression of spontaneous emission rate into the laser mode with respect to that into all modes. The latter can be estimated by assuming interaction with a continuum of modes in a uniform 3D space. The result is reproduced here from ref. 16,

$$W_{sp}^{(all)} \equiv \frac{1}{t_{sp}} = \frac{16\pi^3\mu'^2}{h\epsilon(\bar{r}_a)\,(\lambda/n)^3}, \quad [18]$$

where t_{sp} is the spontaneous radiative lifetime of the emitter and n is the average refractive index of the dielectric medium. Note that the dipole matrix element μ' in Eq. **18** is not the same as that of Eq. **6**. The former accounts for all possible dipole polarizations in the 3D space, whereas the latter accounts only for dipoles parallel to the principal electric field component of the transverse electric-polarized laser mode. They are related through $\mu' = \sqrt{3}\mu$. A Purcell factor for the laser mode (ℓ) can now be defined as the ratio of Eqs. **6–18**,

$$F_p^{(\ell)} = \frac{1}{8\pi}\left(\frac{\lambda}{n}\right)^3 g_a(\nu_\ell)\nu_\ell|\bar{E}_\ell(\bar{r}_a)|^2 = \quad [19]$$

$$= \frac{1}{4\pi^2}\left(\frac{\lambda}{n}\right)^3\frac{\mathrm{Q_a}}{V_{eff,a}}, \quad [20]$$

where $\mathrm{Q_a} = \nu_a/\Delta\nu_a$ is an effective Q factor for a homogeneously broadened resonance centered at $\nu_a \simeq \nu_\ell$, with a full-width at

half-maximum of $\Delta\nu_a = 2[\pi g_a(\nu_a)]^{-1}$, and $V_{eff,a} = |\bar{E}_\ell(\bar{r}_a)|^{-2}$ is a normalized modal volume describing the interaction of the laser mode with the emitter. A factor-of-three aside (due to the restriction to linearly polarized dipoles), Eq. **20** bears the exact notational form as that of Purcell's in the limit where the transition linewidth is much broader than the optical. Recall that because of the quantization normalization Eq. **4**, $|\bar{E}_\ell(\bar{r}_a)|^2$ has dimensions of inverse volume. This shows and quantifies formally the existence of an equivalent volume "lever" for the control of the spontaneous emission into a select mode, wielded not by changing the physical size of the resonator, but by engineering the mode's spatial distribution with respect to the emitter.

Appendix C: Definition of Q_{III-V}. For an optical mode partially overlapping a III-V portion of the cavity, an effective Q factor, Q_{III-V}, can be defined to account for the contribution of loss in the III-V to the overall (i.e., loaded) Q of the resonator. Using the definition

$$Q_{III-V} = \omega_\ell \frac{\text{energy stored in resonator}}{\text{power dissipated in the III}-\text{V}}, \quad [21]$$

and assuming a III-V material with an average, spatially independent optical susceptibility $\chi'(\nu_\ell) - i\chi''(\nu_\ell)$, we have

$$Q_{III-V} = \frac{\int_{V_c} \epsilon_o |\bar{E}_\ell(\bar{r})|^2 d^3\bar{r}}{\int_{V_{III-V}} \epsilon(r)\chi'' |\bar{E}_\ell(\bar{r})|^2 d^3\bar{r}}, \quad [22]$$

where, again, $\bar{E}_\ell(\bar{r})$ is the laser eigenmode function. Substituting in (22) yields

$$Q_{III-V} = \frac{n^2_{III-V}}{\chi''}\left[\int_{V_{III-V}} |\bar{E}_\ell(\bar{r})|^2 d^3\bar{r}\right]^{-1} \equiv \frac{Q^{(b)}_{III-V}}{\Gamma_{III-V}}, \quad [23]$$

where the normalization of Eq. **4** has been implicitly used for the integration over the cavity volume V_c and $Q^{(b)}_{III-V}$ is the absorption-limited Q of the bulk III-V. In the limiting, yet realistic, case, where absorption in the active region accounts for the majority of the III-V loss, Q_{III-V} is formally inversely proportional to $|\bar{E}_\ell(\bar{r}_a)|^2$, setting up a key interdependence between spontaneous emission and loss.

Appendix D: Threshold Current Dependence. There exists an eventual trade-off between spontaneous emission control and threshold current that limits the maximum achievable noise reduction. Here, we derive in a general way an expression for the threshold current to help clarify this relation. We approximate the semiconductor gain medium with an equivalent two-level laser system—that is, one where the lasing action takes place between population-inverted ground (lower) and excited (upper) energy levels. Above threshold and at equilibrium, the rate of net stimulated emission equals that of photon loss. If N_{2t} is the upper-state threshold population and N_{1t} the respective lower-state one, this balance is expressed by

$$(N_{2t} - N_{1t})\, W^{(\ell)}_{st} = \frac{n_\ell}{\tau^{(\ell)}_p}, \quad [24]$$

where $\tau^{(\ell)}_p$ is the cold-cavity photon lifetime of the laser mode. Given the connection between the stimulated and spontaneous emission rates, as expressed by Eq. **7**, we have

$$N_{2t}\, W^{(\ell)}_{sp} = \frac{\eta}{\tau^{(\ell)}_p} = \eta\frac{\omega_\ell}{Q}, \quad [25]$$

where η is the population inversion factor, defined as $\eta = N_{2t}/(N_{2t} - N_{1t})$. Eq. **25** expresses a fundamental balance; assuming fixed Q and inversion, any change in the rate of spontaneous emission, $W^{(\ell)}_{sp}$, has to be accompanied by an equal change of opposite sign in the upper-state threshold population, N_{2t}.

This balance can be reformulated by means of an effective threshold current (actual electric current in the case of an electrically pumped semiconductor laser) as

$$I_{th} \equiv \frac{eN_{2t}}{t_{sp}} = \frac{8\pi^3 e\eta\Delta\nu_a}{|\bar{E}_\ell(\bar{r}_a)|^2 Q\,(\lambda/n)^3}, \quad [26]$$

where the total spontaneous emission lifetime, t_{sp}, as derived in Eq. **18**, has been used. The key result here is the appearance of the product $|\bar{E}_\ell(\bar{r}_a)|^2 Q$ in the denominator. For a laser with sufficiently high Q_{Si}, there exist two distinct limiting regimes: one where the total loss is limited by loss in the III-V and one limited by loss in Si. In the former regime, $Q \simeq Q_{III-V}$ and given that Q_{III-V} is inversely proportional to $|\bar{E}_\ell(\bar{r}_a)|^2$, as shown in *Appendix C*, the product $|\bar{E}_\ell(\bar{r}_a)|^2 Q$ is essentially a constant, and so is the threshold current. This holds up to the point where $Q_{III-V} \simeq Q_{Si}$, beyond which the threshold begins to increase, as illustrated graphically in Fig. 3*B*. Obviously, the higher Q_{Si}, the larger the available penalty-free margin for noise reduction.

Appendix E: Upper-State Threshold Carrier Population and Stored Photon Number. From the laser threshold condition we have

$$g_{th} = \frac{\omega_\ell}{|\bar{E}_\ell(\bar{r}_a)|^2\, V_a Q}, \quad [27]$$

where g_{th} is a temporal, threshold material gain coefficient (in s^{-1}) constant at threshold, V_a is the volume of the active region, and Q is the loaded Q factor of the resonator. For simplicity, but without loss of generality, we have taken the modal intensity as constant over the relatively "thin" active region. In a well-designed laser—that is, a laser oscillating far from gain saturation—the gain can be approximated as a linear function of the carrier density (25),

$$g_{th} = g'(N_{2t} - N_{tr}), \quad [28]$$

where g' is a material-dependent, differential gain coefficient (in s^{-1}) and N_{2t} and N_{tr} are the absolute, upper-state threshold and transparency carrier populations, respectively. The number of photons stored in the laser mode above threshold is given by

$$n_\ell = \eta_i \frac{I - I_{th}}{e}\frac{Q}{\omega_\ell}. \quad [29]$$

From Eqs. **27–29**, we acquire the upper-state carrier population N_{2t} and photon number n_ℓ to substitute in Eq. **1**.

Materials and Methods

Device Fabrication. The optical guiding and frequency-selecting elements (i.e., waveguide and grating) of the lasers of this work are fabricated on a Si-on-insulator (SOI) platform with a 500-nm- and 1 μm-thick Si and buried SiO_2 layer, respectively. The precursor to the SiO_2 QNCL, used for the control of spontaneous emission into the laser mode, is grown first by dry thermal oxidation of an initially thicker Si layer. Control of the final QNCL thickness with nanometer precision is achieved with timed, wet-etch thinning in buffered hydrofluoric acid. Device patterning on Si is carried out by electron beam lithography and a two-step plasma etch. The pattern is transferred first into a 20-nm chromium (Cr) mask by Cl_2/O_2 plasma and subsequently through the QNCL and partially into Si with a C_4F_8/O_2 chemistry.

A 5×QW (InGaAsP, $\lambda_{PL} = 1.55$ μm) III-V die is transferred n-side down onto the patterned SOI chip via direct bonding. The Si and III-V chips are cleaned before bonding by wet chemical treatment and oxygen plasma in succession, the latter also activating the two surfaces for bonding. The two chips are bonded, first manually in ambient environment and then in vacuum for 5 h at a 285 °C plate temperature and while being pressed together under 225-mbar pressure. Following bonding, the InP substrate is

APPLIED PHYSICAL SCIENCES

removed by wet etching. A low-resistance current path is defined in the III-V by proton (H^+) implantation. A Ti/Pt/Au p-metal stack is electron-beam evaporated and patterned by lift-off, followed by a mesa definition by wet etching down to the n-InP contact layer. A Ge/Au/Ni/Au n-metal stack is then evaporated and patterned. The contacts are annealed at 280 °C, and the chip is finally lapped, cleaved in bars, and antireflection-coated for testing.

Frequency Noise Measurement. For the measurement of the laser frequency noise spectrum, we use a short Mach–Zehnder interferometer (MZI; 1.6-GHz free-spectral range), biased at quadrature as a frequency discriminator. To minimize external noise injection, we use a battery-powered, ultra-low-noise current source to drive the laser. The laser output is coupled into a lensed fiber with coupling loss of ∼4–6 dB, amplified by an EDFA to raise the signal level above that of the detector's noise floor, and launched into the input port of the MZI, one arm of which is piezo-controlled. The two outputs of the MZI are connected to a pair of couplers that couple 5% and 95% of the light to a slow and a fast (23 GHz bandwidth) balanced photodetector (PD), respectively. The input fibers to the balanced PDs are length-matched to within 1 mm for maximal intensity noise rejection. The slow-balanced PD is connected to an electronic feedback circuit board that locks the MZI via the piezo in quadrature. The fast-balanced PD is connected to a radio frequency spectrum analyzer, and the resulting spectrum is postprocessed to obtain the calibrated frequency noise spectrum.

ACKNOWLEDGMENTS. We thank the Kavli Nanoscience Institute at Caltech for critical support and infrastructure. This work was supported by the Army Research Office and the Defense Advanced Research Projects Agency.

1. Schawlow AL, Townes CH (1958) Infrared and optical masers. *Phys Rev* 112:1940–1949.
2. Henry CH (1982) Theory of the linewidth of semiconductor lasers. *IEEE J Quantum Electron* 18:259–264.
3. Purcell EM (1946) Spontaneous emission probabilities at radio frequencies. *Phys Rev* 69:681–681.
4. Yablonovitch E (1987) Inhibited spontaneous emission in solid-state physics and electronics. *Phys Rev Lett* 58:2059–2062.
5. Vahala KJ (2003) Optical microcavities. *Nature* 424:839–846.
6. Noda S, Fujita M, Asano T (2007) Spontaneous emission control by photonic crystals and nanocavities. *Nat Photon* 1:449–458.
7. Yamamoto Y, Machida S, Björk G (1991) Microcavity semiconductor laser with enhanced spontaneous emission. *Phys Rev A* 44:657–668.
8. Pelton M, et al. (2002) Efficient source of single photons: A single quantum dot in a micropost microcavity. *Phys Rev Lett* 89:233602.
9. Englund D, et al. (2005) Controlling the spontaneous emission rate of single quantum dots in a two-dimensional photonic crystal. *Phys Rev Lett* 95:013904.
10. Agrawal GP, Gray GR (1991) Intensity and phase noise in microcavity surface-emitting semiconductor lasers. *Appl Phys Lett* 59:399–401.
11. Björk G, Karlsson A, Yamamoto Y (1992) On the linewidth of microcavity lasers. *Appl Phys Lett* 60:304–306.
12. Dirac PAM (1927) The quantum theory of the emission and absorption of radiation. *Proc R Soc Lond A Math Phys Eng Sci* 114:243–265.
13. Glauber RJ (2006) Nobel lecture: 100 years of light quanta. *Rev Mod Phys* 78:1267–1278.
14. Ip E, Lau APT, Barros DJF, Kahn JM (2008) Coherent detection in optical fiber systems. *Opt Express* 16:753–791.
15. Slater JC (1946) Microwave electronics. *Rev Mod Phys* 18:441–512.
16. Yariv A (1989) *Quantum Electronics* (Wiley, New York), 3rd ed.
17. Fang AW, et al. (2006) Electrically pumped hybrid AlGaInAs-Silicon evanescent laser. *Opt Express* 14:9203–9210.
18. Akahane Y, Asano T, Song BS, Noda S (2003) High-Q photonic nanocavity in a two-dimensional photonic crystal. *Nature* 425:944–947.
19. Kuramochi E, et al. (2010) Ultrahigh-Q one-dimensional photonic crystal nanocavities with modulated mode-gap barriers on SiO_2 claddings and on air claddings. *Opt Express* 18:15859–15869.
20. Santis CT, Steger ST, Vilenchik Y, Vasilyev A, Yariv A (2014) High-coherence semiconductor lasers based on integral high-Q resonators in hybrid Si/III-V platforms. *Proc Natl Acad Sci USA* 111:2879–2884.
21. Santis C, Yariv A (2015) High-Q silicon resonators for high-coherence hybrid Si/III-V semiconductor lasers. *CLEO: Science and Innovations 2015, San Jose, CA* (Optical Society of America, Washington, DC), SW3F.6.
22. Sysak MN, et al. (2007) Experimental and theoretical thermal analysis of a hybrid silicon evanescent laser. *Opt Express* 15:15041–15046.
23. Vilenchik Y, Santis CT, Steger ST, Satyan N, Yariv A (2015) Theory and observation on non-linear effects limiting the coherence properties of high-Q hybrid Si/III-V lasers. *Conference on Novel In-Plane Semiconductor Lasers XIV, San Francisco, CA, February 9-12, 2015*. *Proceedings of SPIE* (Society of Photo-Optical Instrumentation Engineers, Bellingham, WA), 9328.
24. Vilenchik Y (2015) Narrow-linewidth Si/III-V lasers: A study of laser dynamics and nonlinear effects. PhD thesis (California Institute of Technology, Pasadena, CA).
25. Coldren LA, Corzine SW, Masanovic ML (2012) *Diode Lasers and Photonic Integrated Circuits* (Wiley, New York), 2nd ed.